Influence of LC Content on the Phase Structures of Side-Chain Liquid Crystalline Block Copolymers with Bent-Core Mesogens

Kishore K. Tenneti,[†] Xiaofang Chen,*[,‡] Christopher Y. Li,*[,†] Zhihao Shen,[‡] Xinhua Wan,[‡] Xinghe Fan,[‡] Qi-Feng Zhou,*[,‡] Lixia Rong,[§] and Benjamin S. Hsiao[§]

A. J. Drexel Nanotechnology Institute and Department of Materials Science and Engineering, Drexel University, Philadelphia Pennsylvania 19104, Department of Polymer Science and Engineering and The Key Laboratory of Polymer Chemistry and Physics of Ministry of Education, College of Chemistry, Peking University, Beijing 100871, P. R. China, Department of Chemistry, Stony Brook University, Stony Brook, New York 11794

Received December 10, 2008; Revised Manuscript Received March 8, 2009

ABSTRACT: We report the phase structures of a series of poly(styrene-*block*-{3′-[4-(4-*n*-dodecyloxybenzoyloxy)benzoyloxy]-4-(12-methacryloyloxydodecyloxy)benzoyloxybiphenyl}) (PS-*b*-PMAC) side-chain liquid crystalline block copolymers (SC LCBCP). The SC liquid crystalline polymer was formed by side attaching a bent-core mesogen to the polymer backbone using a 12-carbon spacer. The phase structure of the high and low f^{PMAC} samples were investigated using differential scanning calorimetry, small-angle and wide-angle X-ray scattering, and transmission electron microscopy techniques. The PS coil block and PMAC LC block phase separate into a lamellar morphology in all of the samples investigated (volume fraction of PMAC $f^{PMAC} \sim 0.31-0.65$). However, both the LC phase and the orientation of the hierarchical structure under mechanical shear showed strong dependence on the LC content. Samples having a high f^{PMAC} (0.5−0.65) showed a SmC_2 LC phase (Smectic C denotes the LC molecules are tilted with respect to the layer normal, and 2 represents a bilayered structure), similar to that observed in PMAC homopolymers. Upon mechanical shear, these smectic layers oriented parallel to the shear plane and the BCP lamellae oriented perpendicular to the shear plane with the layer normal parallel to the vorticity direction. In samples having a lower f^{PMAC}, the BCP lamellae laid parallel to the shear plane and the LC phase structure in these samples was columnar rectangular. A detailed structural and morphological study will be reported.

Introduction

Research on block copolymer (BCP) self-assembly has contributed immensely to the development of nanoscale science and technology. BCPs possess inherent ability to form ordered molecular architectures at the length scales varying from 10−100 nm. A variety of highly ordered structures such as lamellae, gyroids, cylinders, and spheres can be obtained with relative ease and high level of control.[1−3] The thermodynamic factors that influence the phase behavior of coil−coil BCPs were systematically investigated.[1−3] With the improving understanding of the fundamentals of BCP phase separation, BCPs are now widely used as templates to achieve multifunctional hierarchical structures for nanotechnology applications. By using a functional segment as one of the blocks in a BCP, additional functionality can be introduced into this system. To this end, liquid crystalline BCPs (LCBCPs) have been obtained by incorporating a LC block in a BCP.[4] Because LCs self-assemble into 1D and 2D nanostructures at 1−10 nm[5,6] and this length scale is 1 order of magnitude smaller than that offered by the BCP phase separation, thus hierarchical structures can be realized in LCBCPs. In addition, intriguing phase behavior has been observed in these materials because the final structure formation is driven by two competing processes: BCP microphase separation and LC ordering. BCP phase separation creates a large scale, ordered "scaffold" where LC ordering takes place in the confined BCP domain within the scaffold. These two processes compete with each other and the final phase morphology is dictated by whichever the dominant process is. This competition concept was clearly demonstrated in rod−coil BCP (RCBCP) systems where one segment of the BCP adopts an extended rodlike conformation where these rods are considered as (macromolecular) mesogens. Main-chain LC, polypeptide, polyisocynate deritives,[7−11] and mesogen-jacketed LCPs have been used as the rod segments.[12−15] The rigid macromolecular mesogens impart a rodlike character to the polymer backbone and enhance the incompatibility between the blocks. The LC ordering induced by the macromolecular mesogens, in general, is a much stronger physical process because of the combination of strong intermolecular interactions and the enthalpic penalty associated with the bending modulus of the rigid rod molecules. LC ordering thus overwhelms BCP phase separation and, even at extremely asymmetric volume fractions, curved intermaterial dividing surfaces (IMDS) (such as those in gyroids and spheres BCP cases) are rarely observed in these RCBCPs. The compromise between asymmetric volume fraction of BCPs and the rigid rod nature of one segment results in many interesting phase morphologies (such as arrowhead, zigzag lamellae, perforated layered structures) at asymmetric volume fractions.[7,13] Recently, our group has demonstrated that, by introducing a soft shell around the rigid rod and synthesizing core−shell rods, LC interaction between the rods was weakened. In such core−shell RCBCP systems, BCP phase separation could become the dominant process and phase morphology with highly curved IMDS was obtained in asymmetric samples.[16,17] Furthermore, the nanodomains with curved interfaces destabilized LC ordering. Thus, the competition between BCP phase separation and LC ordering is subtle and its effect on the final phase morphology is profound.

This type of competition process is less significant in side chain (SC) LCBCP where LC mesogens are linked to the BCP backbones at the end of the mesogen via a soft spacer.[4,18−33]

* To whom correspondence should be addressed. Tel: 215-895-2083. Fax: 215-895-6760. E-mail: chrisli@drexel.edu (C.L), E-mail: chenxiaofang@pku.edu.cn (X.C.), Tel: 86-10-62756660. E-mail: qfzhou@pku.edu.cn (Q.-F.Z.).
[†] Drexel University.
[‡] Peking University.
[§] Stony Brook University.

10.1021/ma8027563 CCC: $40.75
Published on Web 04/20/2009

Scheme 1. (a) Synthetic Route for Poly(styrene-*block*-{3′-[4-(4-*n*dodecyloxybenzoyloxy) benzoyloxy]-4-(12-methacryloyloxydodecyloxy)benzoyloxybiphenyl}) Block Copolymers and (b) ^{1}H NMR of Poly(styrene-*block*-{3′-[4-(4-*n*dodecyloxybenzoyloxy) benzoyloxy]-4-(12-methacryloyloxydodecyloxy)benzoyloxybiphenyl}) with CD_2Cl_2 as Solvent

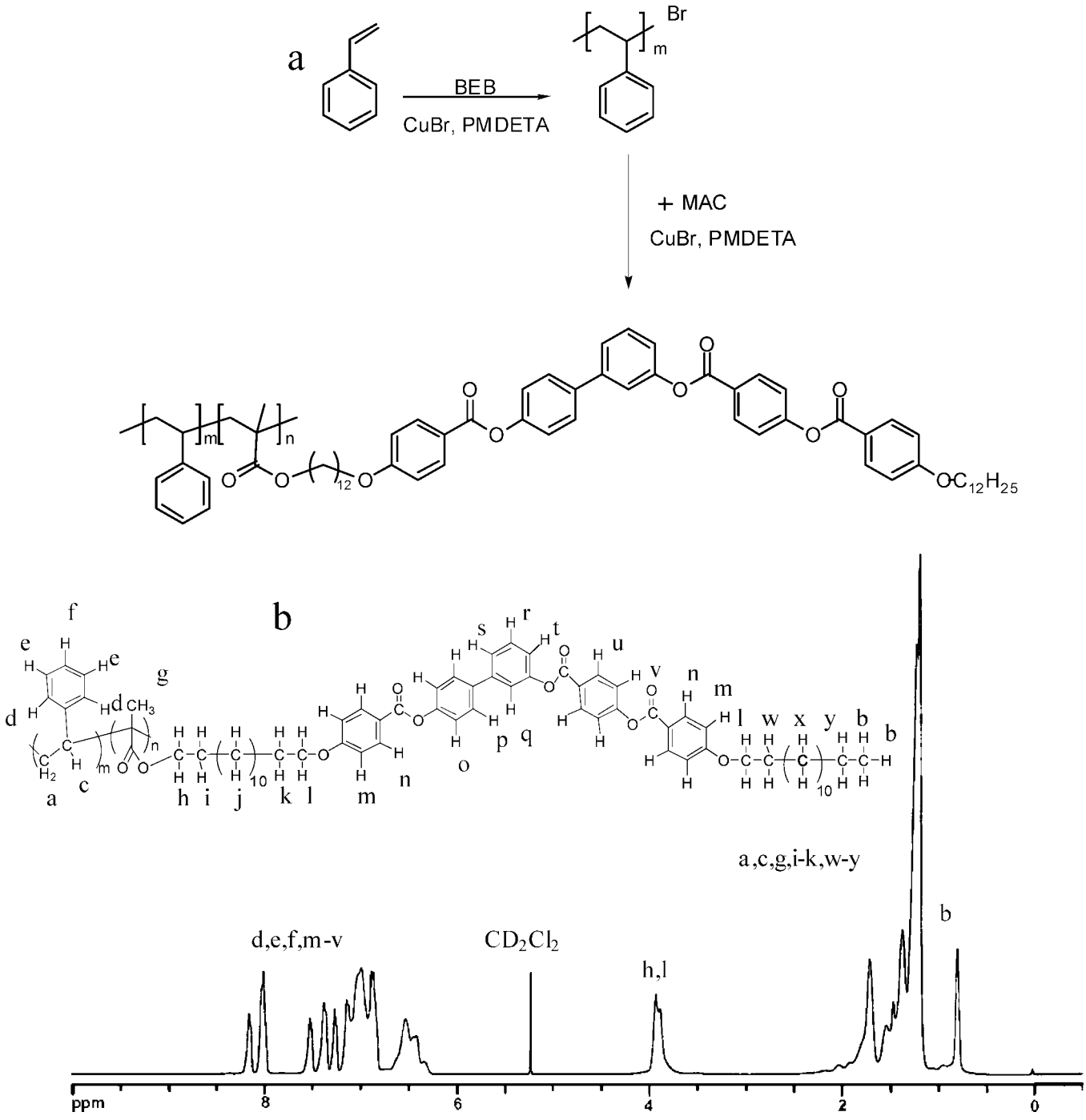

Covalent and noncovalent[34−41] bonds have been used to link LC mesogens to the polymer backbone. The spacer decouples the strong influence of the mesogens on the polymer backbone and it showed an immense impact on the phase behavior of such systems. Unlike RCBCP, conventional phase structures, similar to those observed in the coil−coil systems, were observed in SC-LCBCPs. A variety of SC-LCBCP systems were investigated with cholesteryl-, biphenyl benzoate core-, biphenyl ester core-, fluorinated-, and azobenzene-based LC mesogens side-attached to butadiene-, methacrylate-, isoprene-, and siloxane-based polymers.[4,18−41] Conventional BCP structures such as lamellae, cylinders, and spheres were observed in these samples. The LC phase was predominantly smectic (both SmA and SmC*) in the case of lamella- and cylinder-forming systems, whereas nematic LC phases were observed at highly asymmetric volume fractions. The interplay between BCP phase structure and LC ordering has also been discussed.

In this article, we report the phase structures of poly(styrene-*block*-{3′-[4-(4-*n*-dodecyloxybenzoyloxy)benzoyloxy]-4-(12-methacryloyloxydodecyloxy)benzoyloxybiphenyl}) (PS-*b*-PMAC) SC-LCBCPs as shown in part a of Scheme 1. The PS-*b*-PMAC system contains a bent-core mesogen that is attached to a polymethacrylate-based polymer backbone using a 12-carbon alkyl spacer. PMAC forms the LC block, whereas PS forms the coil block. Bent-core mesogens are chosen because they exhibit interesting phase structures and excellent electro-

Table 1. Molecular Analysis of Poly(styrene-*block*-{3′-[4-(4-*n*-dodecyloxybenzoyloxy)-benzoyloxy]-4-(12-methacryloyloxydodecyloxy)benzoyloxybiphenyl}) Block Copolymers

sample	Mn (PS)	Mn(PMAC)	total Mn	f^{PMAC}
		High f^{PMAC}		
PS_{212}-*b*-$PMAC_{62}$	22 000	50 400	72 400	0.65
PS_{192}-*b*-$PMAC_{39}$	20 000	31 800	51 800	0.56
PS_{212}-*b*-$PMAC_{34}$	22 000	27 300	49 300	0.50
		Low f^{PMAC}		
PS_{212}-*b*-$PMAC_{20}$	22 000	16 200	38 200	0.37
PS_{212}-*b*-$PMAC_{15}$	22 000	12 100	34 100	0.31

optical properties.[42−47] The influence of the f^{PMAC} (volume fraction) on the overall BCP morphology was investigated by varying f^{PMAC} between 0.31 and 0.65. On the basis of f^{PMAC}, the BCP samples are categorized as high f^{PMAC} (0.5−0.65) and low f^{PMAC} (0.31−0.37) samples and their characteristics are listed in Table 1. BCP lamellar phase was formed in all of the samples. However, depending upon f^{PMAC}, the PMAC mesogens form different LC phases. Samples having a high f^{PMAC} formed a bilayered SmC_2 (Smectic C denotes the LC molecules are tilted with respect to the layer normal, and 2 represents a bilayered structure) LC phase (similar to that observed in homopolymer PMAC[45]) and in low f^{PMAC} samples, columnar rectangular (Φ_R) LC phase was observed. These BCPs also respond differently to mechanical shear. The difference was attributed to the competition between BCP phase separation and LC ordering.

Experimental Section

Materials. Styrene was purchased from Beijing Chemical Company and was distilled over calcium hydride. Chlorobenzene was purified by washing with concentrated sulfuric acid to remove thiophene, followed by washing with water, and then dried and distilled. *N*,*N*,*N*′,*N*″,*N*″′-Pentamethyldiethylenetriamine (PMDETA) (>98%, TCI) and 1-bromoethylbenzene (BEB) (97%, Acros) were used as received without further purification. Cuprous bromide (CuBr) was purified by stirring in glacial acetic acid, filtering, and washing with ethanol and was then dried under vacuum.

Diblock Copolymer Synthesis. The chemical structure and synthesis of the polymer are shown in part a of Scheme 1. All BCPs were synthesized by sequential atom transfer radical polymerization (ATRP).

Synthesis of PS-Br Macroinitiators. Macroinitiator PS-Br was synthesized as follows. Typically, styrene (8.012 g, 0.077 mol), BEB (0.041 g, 0.22 mmol), and PMDETA (0.038 g, 0.22 mmol) were added sequentially into a 50 mL reaction tube containing a magnetic stir bar. The reaction mixture was purged with nitrogen and was subjected to two freeze−thaw cycles to remove any dissolved oxygen. CuBr (0.031 g, 0.22 mmol) was then added into the reaction tube. After another two freeze−thaw cycles, the tube was sealed under vacuum. Polymerization was carried out at 90 °C for 4−5 h. After the polymerization was terminated by immersing the tube into ice/water mixture, the tube was broken. The polymerization mixture was then diluted with 20 mL of THF and was passed through a basic Al_2O_3 column to remove the copper complex. The collected polymer solution was precipitated into methanol. The precipitate was dried under vacuum. The molecular weight and polydispersity of macroinitiators were measured by GPC with PS standards.

Synthesis of PS-*b*-PMAC. PS-*b*-PMAC BCPs were synthesized as follows. Typically, PMAC monomer (0.49 g, 0.51 mmol), PSt-Br (0.23 g, 0.008 mmol), PMDETA (0.0014 g, 0.008 mmol), and chlorobenzene (1.0 g) were added sequentially into a 10 mL reaction tube containing a magnetic stir bar. The reaction mixture was purged with nitrogen and subjected to two freeze−thaw cycles to remove any dissolved oxygen. CuBr (0.0011 g, 0.008 mmol) was added into the reaction tube. After another two freeze−thaw cycles, the tube was sealed under vacuum. The tube was put into an oil bath preset at 90 °C. After the polymerization was terminated by immersing the tube into ice/water mixture, the tube was broken. The polymerization mixture was then diluted with 5 mL of THF and passed through a basic Al_2O_3 column to remove copper complex. After removing the solvent, the product was purified using column chromatography with dichloromethane as the eluent to remove unreacted monomers. It was then concentrated and precipitated into a large amount of methanol. The crude product was collected, and then Soxhlet extracted using cyclohexane to remove unreacted PS. The removal of the monomer from the polymer was confirmed by disappearance of the peaks associated with the vinyl protons at 5.54 and 6.10 ppm in the ^1H NMR spectra of the monomer as shown in part b of Scheme 1. The removal of unreacted PS was confirmed by GPC.

Scheme 2. Schematic Representation of the Shear Geometry

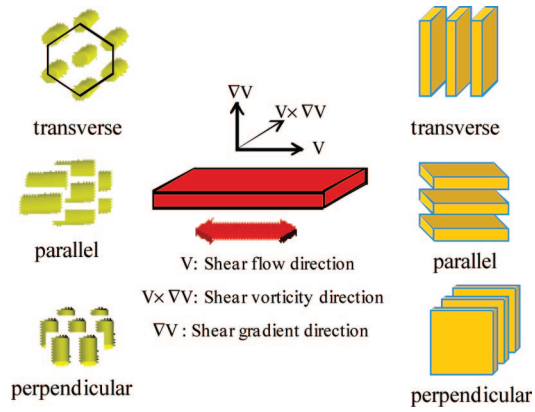

Equipment and Experiments. Sheared polymer samples were obtained by first solution-casting thick polymer films (thickness ~0.5−1 mm) from 5% (w/w) chloroform solutions. The solvent was allowed to evaporate at room temperature for 2 days. Residual solvent was removed under vacuum at 80 °C. The sample was then annealed at 165 °C for 3 days to allow microphase separation. To achieve uniform shear alignment of the microdomains, the microphase-separated samples were subjected to a large-amplitude reciprocating shear at ~165 °C (higher than the isotropization temperature of the LCPs) for 40−60 min. The shear frequency was ~0.5 Hz, and the shear amplitude was ~150%. The shear geometry is shown in Scheme 2. The resultant polymer film was then taken out of the shearing apparatus and quenched to room temperature. The samples were annealed at ~165 °C for 1 day to release residual shear stress. The final film thickness was ~0.2−0.3 mm.

Differential scanning calorimetry (DSC), small-angle X-ray scattering (SAXS), wide-angle X-ray diffraction (WAXD), and transmission electron microscopy (TEM) were used to characterize the structure and morphology of the BCPs. The thermal transitions were detected using a PerkinElmer DSC-7. The temperature and heat flow were calibrated using standard materials at different cooling and heating rates between 5 and 40 °C/min. Samples with a typical mass of 3 mg were encapsulated in sealed aluminum pans. A controlled cooling experiment was always carried out first, and a subsequent heating run was performed at a rate that was equal to or faster than the previous cooling. 2D SAXS experiments were carried out at the synchrotron X-ray beamline X-27C at the National Synchrotron Light Source in Brookhaven National Laboratory. The sample−detector distance of the 2D SAXS setup was calibrated using silver behenate, with the first-order scattering vector q being 1.076 nm^{-1}. The air scattering for WAXD was subtracted. The X-ray beam spot was ~0.1 mm in diameter. 2D WAXD patterns were also recorded at room temperature in the same set up with the sample to detector distance of ~15−19 cm.

TEM experiments were conducted using a JEOL 2000FX TEM with an accelerating voltage of 120 kV. A Reichert Ultracut cryo-ultramicrotome was used to microtome the sheared BCP sample.

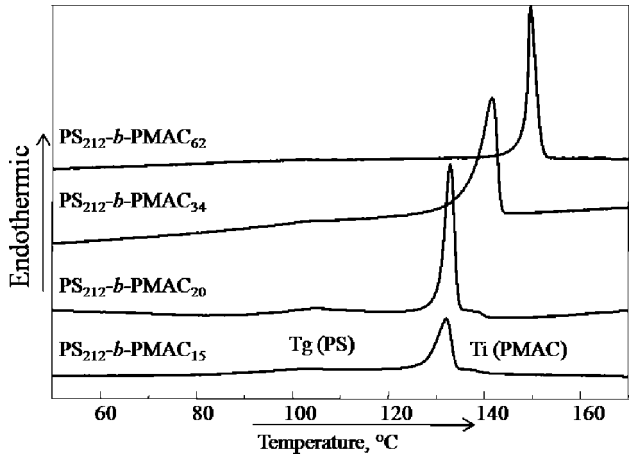

Figure 1. Representative differential scanning calorimetry plots of symmetric and asymmetric poly(styrene-*block*-{3′-[4-(4-*n*-dodecyloxybenzoyloxy)benzoyloxy]-4-(12-methacryloyloxydodecyloxy)benzoyloxybiphenyl}) block copolymers.

Thin sections of the BCP (~50 nm thick) were obtained at room temperature and were collected on nickel TEM grids, followed by staining in ruthenium tetroxide (RuO_4) vapor for approximately 40 min.

Results and Discussion

Phase Behavior of High f^{PMAC} PS-*b*-PMAC. Figure 1 shows representative endothermic DSC plots of PS-*b*-PMAC samples obtained with a heating rate of 10 °C/min. The glass transition of PS and the LC melt transition temperature (T_{LC-I}) of PMAC are evident from the plots. Note that with increasing f^{PMAC}, T_{LC-I} increased from ~130 to 152 °C. Details about this temperature change will be discussed in the following section. Microphase separated samples were subjected to reciprocating mechanical shear to obtain uniformly aligned morphology. The shear geometry is shown in Scheme 2. V, V × ∇V, and ∇V indicate shear flow, shear vorticity, and shear gradient directions, respectively. Parts a and b of Figure 2 show the 2D SAXS pattern of PS_{212}-*b*-$PMAC_{62}$ of the V × ∇V/∇V and V × ∇V/V planes, respectively. In part a of Figure 2, scattering peaks possessing a ratio of 1:2 can be clearly seen along the meridian direction and the *d*-spacing of the primary scattering peak is ~50.2 nm, suggesting a simple lamellar BCP structure. Part c of Figure 2 shows the WAXD pattern of the same sample of the V × ∇V/∇V plane. Note that the same pattern can be found for the WAXD of V /∇V plane. Along the equatorial direction, about six orders of scattering peaks, possessing a 1:2:3:4:5:6 ratio with respect to the primary peak, are evident and the *d*-spacing of the primary scattering peak is ~8.1 nm. This indicates the presence of a layered smectic type of LC phase. The azimuthal integration of the amorphous halo in the wide-angle region of the 2D WAXD pattern (part d of Figure 2) shows diffuse arcs symmetrically placed about the meridian forming pairs of straight lines at an angle of ~46° from the meridian, suggesting a SmC type LC phase, where the mesogens are tilted with respect to the layer normal. On the basis of the *d*-spacing of the primary peak obtained from the WAXD pattern and the previous studies, a bilayered SmC_2, similar to that observed in the case of PMAC homopolymers, can be confirmed.[44,46,48−50] The hierarchical structure thus is SmC_2-in-L.

Figure 3 shows the TEM image of PS_{212}-*b*-$PMAC_{62}$ of the V × ∇V/∇V plane. Similar morphology was obtained for the V × ∇V/V plane. Thin sections of ~50 nm were microtomed and stained in RuO_4 vapors for ~40 min to enhance the contrast between the two blocks. Because RuO_4 selectively stains PS, the dark domains are the PS lamellae and the bright layers are PMAC. An interesting observation from the X-ray scattering and TEM data is the orientation of the BCP lamellae with respect to the shear geometry. Generally, in a simple lamellar coil−coil BCP system oriented using mechanical shear, the preferred orientation of the BCP lamellae is parallel to the shear plane (V/V × ∇V). In such a case, the SAXS pattern along the V × ∇V zone and V zone should possess lamellar scattering and they should be located along the equatorial direction as per our experimental setup. However, the lamellar scatterings in our case were observed along the meridian in the V × ∇V/∇V plane and no scatterings were observed in the V/∇V plane. In addition, the appearance of lamellar scatterings along the meridian direction of the V/V × ∇V plane further suggests that the BCP lamellae are not oriented parallel to the V/V × ∇V plane; instead, they are oriented perpendicular to the V/V × ∇V plane with the layer normal parallel to the V × ∇V. From the WAXD results (part c of Figure 2), the LC diffractions are located along the equatorial direction. The orthogonal orientation of the smectic LC layer diffractions and the BCP lamellar scatterings indicates that the smectic layers are oriented perpendicular to the BCP interface. On the basis of the X-ray scattering and TEM results, the hierarchical nanostructure of the high f^{PMAC} samples can be constructed and is shown in Figure 4. Accordingly, the PS and PMAC layers undergo microphase separation and form alternating layers and their normals align parallel to V × ∇V upon shear. Within the PMAC layers, the side-chain mesogens and the polymer backbone further undergo phase separation and the mesogens form a bilayered SmC_2 LC phase similar to that observed in PMAC homopolymers.

Phase Behavior of Low f^{PMAC} Samples. Parts a and b of Figure 5 show the SAXS patterns of the V/∇V and V × ∇V/∇V planes obtained from PS_{212}-*b*-$PMAC_{20}$ with an f^{PMAC} of ~37%, which is lower than that of the samples previously discussed. Up to four orders of scattering arcs are clearly visible along the equator and these arcs possess a ratio of 1:2:3:4 with respect to the primary scattering peak, (d = ~37.4 nm) suggesting the formation of a simple lamellar BCP morphology with a layer thickness of ~37.4 nm. Of interest is the orientation of these BCP lamellae with respect to the shear geometry. In contrast to the X-ray results observed in the high f^{PMAC} samples, the lamellar scattering arcs are located along the equator when the X-ray beam is parallel to the V × ∇V or V. This indicates that, compared with PS_{212}-*b*-$PMAC_{62}$ previously discussed, the orientation of BCP lamellae has changed and in the PS_{212}-*b*-$PMAC_{20}$ case, they are parallel to the V/V × ∇V plane. A similar BCP orientation was also observed in PS_{212}-*b*-$PMAC_{15}$. WAXD experiments were conducted in order to understand LC orientation and the results are shown in parts c and d of Figure 5 when the X-rays are along the V × ∇V and V directions, respectively. Up to four orders of diffraction arcs are clearly seen along the meridian direction in both figures. These arcs possess a ratio of 1:1.22:2.1 with respect to the primary diffraction peak (q = ~1.57 nm^{-1}). This suggests that the layered smectic LC phase observed in the high LC content samples disappears. The *d*-spacing corresponding to the primary diffraction arc is ~4 nm, which is approximately half of the smectic layer thickness in SmC_2. The ratio between the diffractions reveals that the LC phase present in this sample resembles a Φ_R phase and the diffraction arcs were indexed as (11), (02), and (13), respectively. This assignment is consistent with the previous reports.[44,46,48−50] The lattice parameters are calculated to be a = 5.05 nm and b = 6.56 nm. The position of the diffraction arcs in the WAXD results suggests that these LC columns were oriented parallel to the BCP lamellar normal. Both samples with a low f^{PMAC} (0.31 and 0.037) showed similar LC phase behavior. The hierarchical structure in these samples

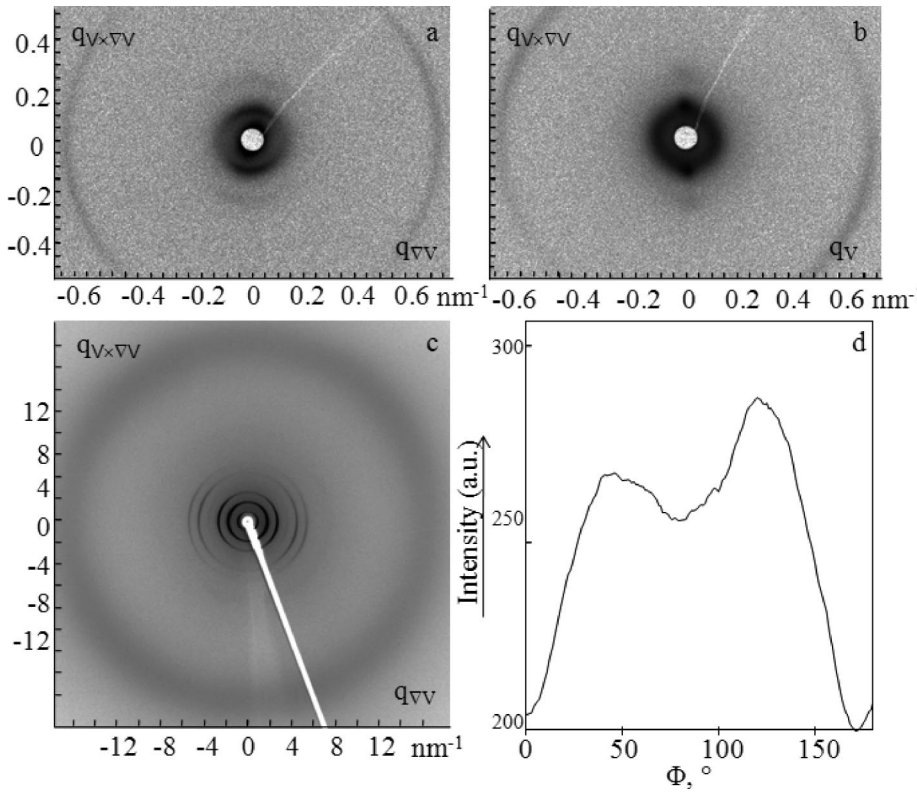

Figure 2. 2D small-angle X-ray scattering pattern of PS_{212}-*b*-$PMAC_{62}$ with the X-rays along the a) shear flow direction (V) and b) shear gradient direction (∇V) as defined in Scheme 2. (c) Wide-angle X-ray diffraction pattern of PS_{212}-*b*-$PMAC_{62}$ obtained along shear vorticity/shear gradient (V × ∇V/∇V) plane. (d) Azimuthal integration of the amorphous halo of (c).

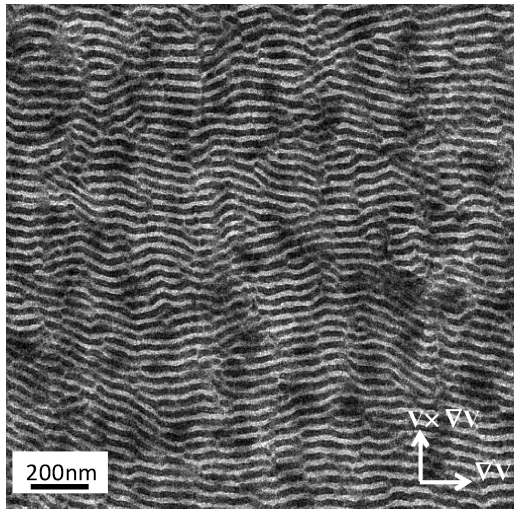

Figure 3. Transmission electron micrograph of PS_{212}-*b*-$PMAC_{62}$ showing the V × ∇V/∇V plane. A similar pattern is obtained along the V × ∇V/V plane.

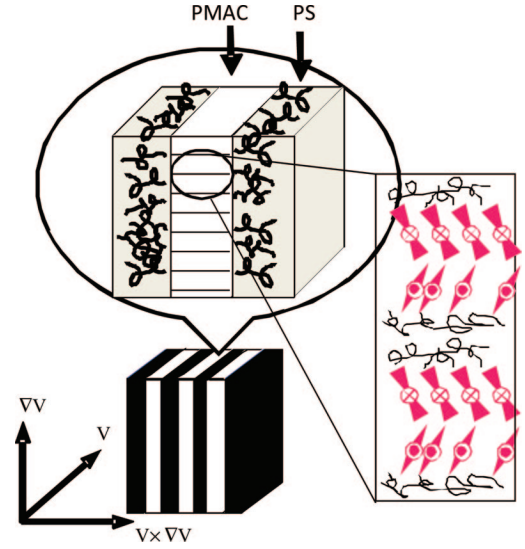

Figure 4. Schematic representation of the phase structures observed in the high f^{PMAC} poly(styrene-*block*-{3′-[4-(4-*n*-dodecyloxybenzoyloxy)benzoyloxy]-4-(12-methacryloyloxydodecyloxy)benzoyloxybiphenyl}) block copolymers.

is thus Φ_R-in-L. Figure 6 shows the TEM micrograph obtained from a 50 nm thick section of the V/∇V plane of the BCP. The section is stained with RuO_4 vapors and the alternating dark and bright stripes represent PS and PMAC lamellae, respectively. A similar image is obtained along the V × ∇V/∇V plane. On the basis of the X-ray scattering and TEM results, the hierarchical phase structures of the low f^{PMAC} samples can be constructed and is shown in Figure 7. Because of the symmetric composition of both the blocks, PS and PMAC form lamellar structures and these lamellae orient parallel to the V/V × ∇V plane. Within the PMAC layers, the side-chain mesogens stack together forming columnar structures with rectangular in-plane symmetry.

Discussion

Competition between BCP phase separation and the LC ordering has been discussed in a number of publications. In our present experiment, the high f^{PMAC} samples adopted a SmC_2-in-L hierarchical structure, whereas the low f^{PMAC} samples possessed a Φ_R-in-L structure. The intriguing feature of our observation is 2-fold: 1) as f^{PMAC} changes from 0.65 to 0.31, although the BCP morphology remained lamellae, the LC ordering changed from SmC_2 to Φ_R, and 2) upon mechanical shear, the orientation of the hierarchical structure changed

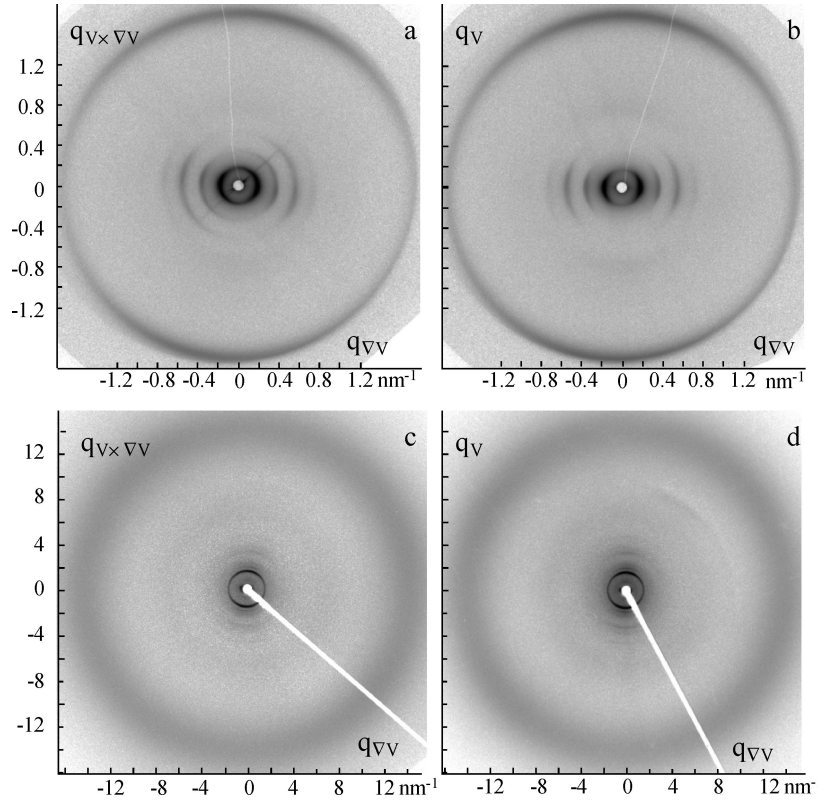

Figure 5. 2D small-angle X-ray scattering pattern of PS_{212}-*b*-$PMAC_{20}$ with the X-rays along a) V and b) V × ∇V as defined in Scheme 2. Wide-angle X-ray diffraction pattern of PS_{212}-*b*-$PMAC_{20}$ with the X-rays along c) V and d) V × ∇V.

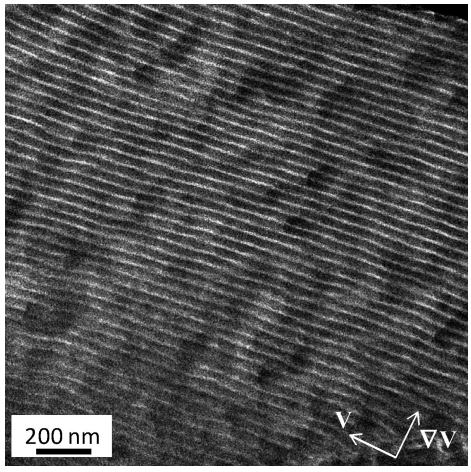

Figure 6. Transmission electron micrograph of PS_{212}-*b*-$PMAC_{20}$ showing the V/∇V plane.

dramatically. To thoroughly understand this unique observation, we first need to confirm if the LC structure change from SmC_2 in homopolymer and high LC containing BCP to Φ_R in low LC containing BCP is because of the mechanical shear effect. To this end, unsheared PS_{212}-*b*-$PMAC_{20}$ sample was subjected to WAXD and the 1D integration of the 2D WAXD result is shown in Figure 8. A strong primary peak ($q = \sim 1.53$ nm^{-1}) and up to three higher order peaks are clearly evident from the figure. The higher order plots possess a ratio of 1:1.22:2.1 with the primary scattering peak, which is the same as that observed in sheared BCP samples. A fourth order peak was also observed and it can be indexed as the (15) diffraction. This indicates that the transformation of PMAC LC phase from SmC_2 to Φ_R upon decreasing LC content is not induced by mechanical shear. Instead, it is a result of the lower LC content. LC ordering change in BCP confined space has been observed in a number of systems. However, in most cases, the LC phase changes from smectic to nematic because of the curved IMDS, which is incompatible with the translational symmetry requirement of the smectic phase. As the BCP domain size decreases, LC becomes increasingly frustrated and the smectic order degenerates into nematic. In the present case, as LC content decreased from 0.65 to 0.31, the lamellar phase was retained and the IMDS therefore remained flat. The LC phase change, therefore, must have been induced by other factors. The possible explanation could be that, because the LC layers become increasingly thinner as the LC content decreases, the in-plane modulation of the LC layer in the smectic phase might destabilize the smectic layer and the layers thus break into columns with the columnar axis parallel to the smectic layer surface. Close packing of the column thus leads to a Φ_R phase.

The second interesting observation is the orientation change of our system upon mechanical shear for lamellar BCPs with slightly different f^{PMAC}. To understand this phenomenon, a brief summary of the BCP/LC behavior under shear is helpful. The behavior of both coil−coil BCP and LC under shear fields have been widely investigated from both theoretical and experimental viewpoints.[51,52] The relative orientation of simple lamellae and cylinder morphologies with respect to shear field is shown in Scheme 2. For lamellae morphology, parallel, transverse, and perpendicular orientations are defined when the lamellar normal is parallel to ∇V, V, and V × ∇V directions, whereas for the cylinder morphology they are defined as the cylinder axis is parallel to the V, V × ∇V, and ∇V directions, respectively. For coil−coil BCPs or smectic-layered LC, it is known that shear flow can align the lamellae with either a parallel or a perpendicular orientation. Much attention has been paid recently to shear-induced orientations in cylinder-forming BCP with LC as the major component. In a PS-*b*-PI system where PI is functionalized with an azobenzene-based mesogen (PI-LC), Ober and Thomas et al. reported the phase behavior as a function

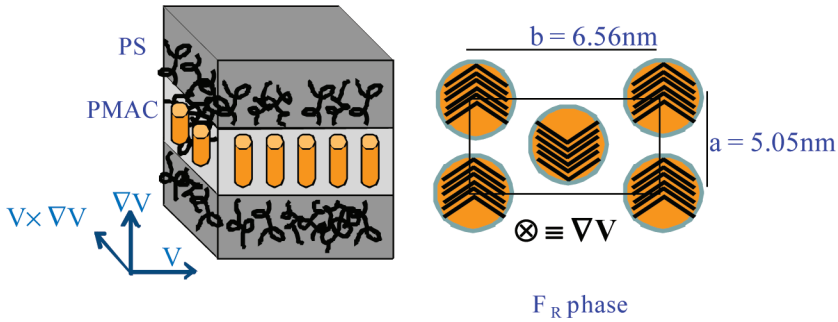

Figure 7. Schematic representation of the phase structures observed in symmetric low f^{PMAC} poly(styrene-*block*-{3′-[4-(4-*n*-dodecyloxybenzoyloxy)-benzoyloxy]-4-(12-methacryloyloxydodecyloxy)benzoyloxybiphenyl}) block copolymers.

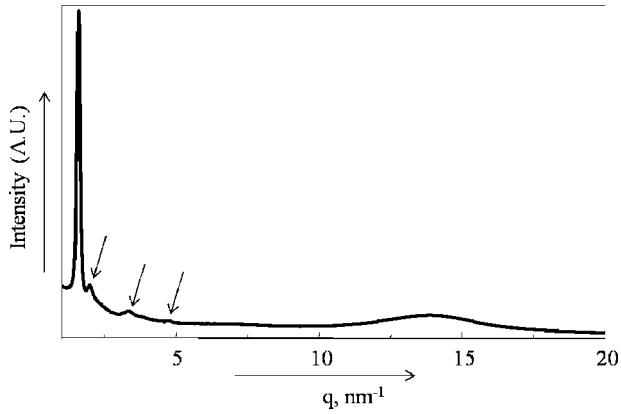

Figure 8. 1D integration of the wide-angle diffraction pattern of unsheared PS_{212}-*b*-$PMAC_{20}$.

of f^{PI-LC} with morphologies including lamellae, PS cylinders in PI-LC matrix, and PI-LC cylinders in PS matrix.[19,21] In shear-oriented cylinder-forming samples where PI-LC formed the majority phase, the authors observed a transformation of the orientation of the cylinders as a function of shearing temperature. When sheared in the smectic LC temperature region, the cylinders adopted a transverse orientation and the smectic layers had a perpendicular orientation. The hierarchical structure can be defined as transverse-perpendicular, the first word indicates the BCP orientation and the second word is the LC orientation. We shall use this notation in the following discussions. Among the possible orientations, the transverse-perpendicular orientation is the most favorable morphology compromise where both the smectic layers and the BCP cylinders are not under strain and this morphology also satisfies the homogeneous anchoring condition of the LCs. In this system, the cylinders reoriented to adopt a parallel orientation (preferred orientation for coil−coil systems) when sheared above the T_I and it was attributed to that the LC phase was not formed during shearing.[24] A similar dominating effect of the LC phase has also been observed in other SC-LCBCP systems. de Jeu et al.[26] reported the bulk and thin film phase behavior of a polymethyl methacrylate (PMMA) and a poly(acrylate) BCP having semifluorinated alkyl side chains that form smectic LC layers. For this type of BCP with $f^{LC} = 0.65$, in thin films, they observed that the smectic layers (matrix) are aligned in a favorable orientation (parallel to the substrate) forcing the orientation of the PMMA cylinders to arrange such that the cylindrical axis is perpendicular to the substrate. They attribute this abnormal cylindrical orientation to the strong influence of the smectic layers formed by the fluorinated side groups (which preferentially wet the substrate and surface).

In our case, it is evident that for high f^{PMAC}, the orientation is perpendicular−parallel, which can be understood considering the competition between BCP and LC ordering under mechanical shear flow. As previously discussed, the most favorable orientation for layer structure under shear is parallel and the second favorable one is perpendicular. In the high f^{PMAC}, because LC is the dominant component, it dictates the most favorable orientation and the BCP has to compromise. Because the BCP and the LC layers are perpendicular to each other in the stable structure, the final orientation of BCP under mechanical shear is perpendicular (as defined in Scheme 2). This orientation is similar to the cylinder-forming LC BCPs with LC as the major component. Note that even in the $f^{PMAC} \sim 0.5$ case, LC dominated the orientation selection. It should also be pointed out that the mechanical shear experiment was conducted at 165 °C, which is ∼10−35 °C higher than the T_{LC-I}. This indicates that, even at temperatures greater than the T_{LC-I}, the influence of the residual LC memory is stronger than that of the BCP, and LC phase structure strongly influences the final orientation in LC BCPs. In a cylinder-forming SC-LCBCP system, Tokita et al.[31] recently reported that, when the LC block is in nemetic phase, the BCP cylinders and the LC director were oriented parallel to V and when the nemetic phase transformed into SmA the cylindrical axis and the LC director orientation changed and they were aligned parallel to ∇V. They attribute this BCP structure transformation to the favorable orientation of the smectic layers parallel to the V/V × ∇V plane. Hammond et al.[25] also recently reported the strong influence of the smectic LC phase: in a PS and poly(vinyl methylsiloxane)-based cylinder-forming SC-LCBCP system with smectic LC layers, PS cylinders adopted transverse orientation and the smectic layer normal was parallel to the cylindrical axis. The cylinders retained their transverse orientation even when the LC was in the isotropic phase although one would expect the cylinders to adopt their favorable orientation (parallel to V) in such a situation. The authors conclude that the LC layers possess residual preferential orientation even in the isotropic state. This LC orientation influence is so strong that it prevents the cylinder reorientation. Our observation is consistent with these recent reports, confirming the strong influence of LC mesogen on the BCP orientation even when the LC is in the isotropic state.

As the LC block content decreases to 0.31 and 0.37, our previous discussion showed that the LC phase changed from SmC_2 to Φ_R. Furthermore, BCP phase separation became the dominant factor in determining the hierarchical structure orientation under mechanical shear: BCP layers adopted the most favorable parallel orientation and the LC columns are perpendicular to the BCP layers, leading to the parallel−perpendicular orientation. Apparently, the influence of the columnar phase on the orientation under shear is not as significant as the LC layered structure. This could be attributed to two reasons: 1) the LC content is less in the columnar LC BCP samples and, therefore, its influence is not as significant, and 2) the column is relatively short because they are confined within BCP layers with the axis parallel to the BCP layer normal, the length of the LC column is on the order of 10−20 nm, and the aspect ratio is only ∼less

than 5. These relatively isotropic rods apparently cannot strongly influence the BCP orientation under shear. Note that the SAXS pattern of the low f^{PMAC} sample (Figure 5) shows higher order than that of the high f^{PMAC} sample (Figure 2) and TEM images also show smoother lamellae for low f^{PMAC}. This can be explained as in the low f^{PMAC} case, BCPs are in the most favorite parallel orientation upon shear, and long-range-ordered, smooth lamellae can be obtained. In the high f^{PMAC} case, upon shear, BCPs are in the least favorite perpendicular orientation. Therefore, poor ordered, corrugated lamellae were observed.

Conclusions

In summary, we report the phase structures of PS-*b*-PMAC SC-LCBCPs that contain a bent-core mesogen. We investigated two types of BCP samples having high and low f^{PMAC}. For all of the samples with f^{PMAC} varying from 0.31 to 0.65, lamellae BCP morphology was observed. The LC phase, however, changed from SmC_2 to Φ_R as the LC content decreased although the IMDS was flat in all the samples investigated. The hierarchical structure was therefore SmC_2-in-L and Φ_R-in-L in high and low f^{PMAC} samples, respectively. The change of the LC phase was attributed to the destabilization of smectic layers as the LC domain size decreased. These two hierarchical structures also responded differently to the shear flow field. For SmC_2-in-L, a perpendicular−parallel orientation was obtained, within which alternating lamellae of PS and PMAC were oriented perpendicular to $V \times \nabla V$ direction, whereas the LC smectic layers were oriented perpendicular to ∇V. This is because LC is the dominant factor in determining the orientation of the hierarchical structures. For Φ_R-in-L, a parallel−perpendicular orientation was adopted where the BCP layers are perpendicular to ∇V and the LC columns are parallel to ∇V. This is because BCP becomes the dominant factor in determining the hierarchical structure. Thus, the competition between BCP phase separation and LC ordering is subtle and its effect on the final phase morphology is profound.

Acknowledgment. This work was supported by the National Science Foundation (NSF CAREER award, DMR-0239415, DMR-0804838), the National Natural Science Foundation of China (No. 20504002), and ACS-PRF. K.K.T. thanks the Ludo Frevel Crystallography Scholarship. Synchrotron experiments were conducted at beamline X27C, NSLS in Brookhaven National Laboratory supported by DOE.

References and Notes

(1) Park, C.; Yoon, J.; Thomas, E. L. *Polymer* **2003**, *44*, 6725–6760.
(2) Bates, F. S. *Science* **1991**, *251*, 898–905.
(3) Bates, F. S.; Fredrickson, G. H. *Annu. Rev. Phys. Chem.* **1990**, *41*, 525–557.
(4) Poser, S.; Fischer, H.; Arnold, M. *Prog. Polym. Sci.* **1998**, *23*, 1337–1379.
(5) de Gennes, P. G. *The Physics of Liquid Crystals*; Chlarendon Press: Oxford, U.K., 1975.
(6) Wang, X. J.; Zhou, Q. F. *Liquid Crystalline Polymers*; World Scientific Publishing Co. Inc.: NJ, 2004.
(7) Chen, J. T.; Thomas, E. L.; Ober, C. K.; Mao, G. P. *Science* **1996**, *273*, 343–346.
(8) Lecommandoux, S.; Achard, M. F.; Langenwalter, J. F.; Klok, H. A. *Macromolecules* **2001**, *34*, 9100–9111.
(9) Stupp, S. I. *Curr. Opin. Colloid Interface Sci.* **1998**, *3*, 20–26.
(10) Olsen, B. D.; Segalman, R. A. *Macromolecules* **2005**, *38*, 10127–10137.
(11) Olsen, B. D.; Segalman, R. A. *Macromolecules* **2006**, *39*, 7078–7083.
(12) Li, C. Y.; Tenneti, K. K.; Zhang, D.; Zhang, H.; Wan, X.; Chen, E.; Zhou, Q.; Avila-Orta, C.; Sics, I.; Hsiao, B. *Macromolecules* **2004**, *37*, 2854–2860.
(13) Tenneti, K. K.; Chen, X. F.; Li, C. Y.; Wan, X.; Zhou, Q. F.; Sics, I.; Hsiao, B. *J. Am. Chem. Soc.* **2005**, *127*, 15481–15490.
(14) Zhou, Q. F.; Zhu, X. L.; Wen, Z. Q. *Macromolecules* **1989**, *22*, 491–493.
(15) Gao, L. C.; Fan, X.; Shen, Z. H.; Chen, X. F.; Zhou, Q. F. *J. Polym. Sci., Part A: Polym. Chem.* **2009**, *47*, 319–330.
(16) Chen, X. F.; Tenneti, K. K.; Li, C. Y.; Bai, Y.; Zhou, R.; Wan, X.; Fan, X.; Zhou, Q. F. *Macromolecules* **2006**, *39*, 517–527.
(17) Tenneti, K. K.; Chen, X. F.; Li, C. Y.; Wan, X.; Fan, X.; Zhou, Q. F.; Rong, L.; Hsiao, B. S. *Soft Matter* **2008**, *4*, 458–461.
(18) Anthamatten, M.; Zheng, W. Y.; Hammond, P. T. *Macromolecules* **1999**, *32*, 4838–4848.
(19) Gallot, B. *Prog. Polym. Sci.* **1996**, *21*, 1035–1088.
(20) Mao, G.; Wang, J.; Clingman, S. R.; Ober, C. K.; Chen, J. T.; Thomas, E. L. *Macromolecules* **1997**, *30*, 2556–2567.
(21) Anthamatten, M.; Hammond, P. T. *Macromolecules* **1999**, *32*, 8066–8076.
(22) Osuji, C.; Zhang, Y.; Mao, G.; Ober, C. K.; Thomas, E. L. *Macromolecules* **1999**, *32*, 7703–7706.
(23) Hamley, I. W.; Castelletto, V.; Lu, Z. B.; Imrie, C. T.; Itoh, T.; Al-Hussein, M. *Macromolecules* **2004**, *37*, 4798–4807.
(24) Osuji, C.; Chen, J. T.; Mao, G.; Ober, C. K.; Thomas, E. L. *Polymer* **2000**, *41*, 8897–8907.
(25) Verploegen, E.; McAfee, L. C.; Tian, L.; Verploegen, D.; Hammond, P. T. *Macromolecules* **2007**, *40*, 777–780.
(26) Al-Hussein, M.; Serero, Y.; Konovalov, O.; Mourran, A.; Moller, M.; de Jeu, W. H. *Macromolecules* **2005**, *38*, 9610–9616.
(27) Walther, M.; Finkelmann, H. *Prog. Polym. Sci.* **1996**, *21*, 951–979.
(28) Ansari, I. A.; Castelletto, V.; Mykhaylyk, T.; Hamley, I. W. *Macromolecules* **2003**, *36*, 8898–8901.
(29) Hamley, I. W. C. V.; Parras, P.; Lu, Z. B.; Imrieb, C. T.; Itoh, T. *Soft Matter* **2005**, *1*, 355–363.
(30) Fischer, H.; Poser, S.; Arnold, M.; Frank, W. *Macromolecules* **1994**, *27*, 7133–7138.
(31) Tokita, M.; Adachi, M.; Masuyama, S.; Takazawa, T.; Watanabe, J. *Macromolecules* **2007**, *40*, 7276–7282.
(32) Zheng, W. Y.; Albalak, R. J.; Hammond, P. T. *Macromolecules* **1998**, *31*, 2686–2689.
(33) Sanger, J.; Gronski, W.; Maas, S.; Stuhn, B.; Heck, B. *Macromolecules* **1997**, *30*, 6783–6787.
(34) Nandan, B.; Lee, C.-H.; Chen, H.-L.; Chen, W.-C. *Macromolecules* **2005**, *38*, 10117–10126.
(35) Valkama, S.; Lehtonen, O.; Lappalainen, K.; Kosonen, H.; Castro, P.; Repo, T.; Torkkeli, M.; Serimaa, R.; ten Brinke, G.; Leskelae, M.; Ikkala, O. *Macromol. Rapid Commun.* **2003**, *24*, 556–560.
(36) Ruokolainen, J.; Makinen, R.; Torkkeli, M.; Makela, T.; Serimaa, R.; Ten Brinke, G.; Ikkala, O. *Science* **1998**, *280*, 557–560.
(37) Brandys, F. A.; Bazuin, C. G. *Chem. Mater.* **1996**, *8*, 83–92.
(38) Ruokolainen, J.; Ten Brinke, G.; Ikkala, O. *Adv. Mater.* **1999**, *11*, 777–780.
(39) Ruokolainen, J. T. J.; ten Brinke, G.; Ikkala, O.; Torkkeli, M.; Serimaa, R. *Macromolecules* **1995**, *28*, 7779–84.
(40) Valkama, S.; Ruotsalainen, T.; Kosonen, H.; Ruokolainen, J.; Torkkeli, M.; Serimaa, R.; ten Brinke, G.; Ikkala, O. *Macromolecules* **2003**, *36*, 3986–3991.
(41) Tenneti, K. K.; Chen, X.; Li, C. Y.; Wan, X.; Fan, X.; Zhou, Q. F.; Rong, L.; Hsiao, B. S. *Macromolecules* **2007**, *40*, 5095–5102.
(42) Coleman, D. A.; Fernsler, J.; Chattham, N.; Nakata, M.; Takanishi, Y.; Korblova, E.; Link, D. R.; Shao, R. F.; Jang, W. G.; Maclennan, J. E.; Mondainn-Monval, O.; Boyer, C.; Weissflog, W.; Pelzl, G.; Chien, L. C.; Zasadzinski, J.; Watanabe, J.; Walba, D. M.; Takezoe, H.; Clark, N. A. *Science* **2003**, *301*, 1204–1211.
(43) Niori, T. S. T.; Watanabe, J.; Furukawa, T.; Takezoe, H. *J. Mater. Chem.* **1996**, *6*, 1231–1233.
(44) Pelzl, G.; Diele, S.; Weissflog, W. *Adv. Mater.* **1999**, *11*, 707–724.
(45) Pelzl, G.; Wirth, I.; Weissflog, W. *Liq. Cryst.* **2001**, *28*, 969–972.
(46) Shen, D.; Pegenau, A.; Diele, S.; Wirt, I.; Tschierske, C. *J. Am. Chem. Soc.* **2000**, *122*, 1593–1601.
(47) Walba, D. M.; Korblova, E.; Shaob, R.; Clark, N. A. *J. Mater. Chem.* **2001**, *11*, 2743–2747.
(48) Chen, X. F.; Tenneti, K. K.; Li, C. Y.; Bai, Y.; Wan, X.; Fan, X.; Zhou, Q. F.; Rong, L.; Hsiao, B. S. *Macromolecules* **2007**, *40*, 840–848.
(49) Shen, D.; Diele, S.; Wirt, I.; Tschierske, C. *Chem Commun.* **1998**, 2573–2574.
(50) Keith, C.; Reddy, R. A.; Baumeister, U.; Tschierske, C. *J. Am. Chem. Soc.* **2004**, *126*, 14312–14313.
(51) Koppi, K. A.; Tirrell, M.; Bates, F. S.; Almdal, K.; Colby, R. H. *J. Phys. II* **1992**, *2*, 1941–1959.
(52) Bruinsma, R.; Rabin, Y. *Phys. Rev. A* **1992**, *45*, 994–1008.

MA8027563